FABRICATION, SELF-ASSEMBLY AND DYNAMICS OF ANISOTROPIC COLLOIDS

Draft of September 17, 2010 at 15 : 33

BY

ADAM DECONINCK

THESIS

Submitted in partial fulfillment of the requirements
for the degree of Master of Science in Materials Science and Engineering
in the Graduate College of the
University of Illinois at Urbana-Champaign, 2010

Urbana, Illinois

Master's Committee:

Professor Jennifer A. Lewis

Abstract

This work details the development of techniques to fabricate and study structured colloidal particles...

To Leigh.

Acknowledgements

Any scientific project which is not completely trivial is the work of many different people, and this project is no exception. First of all I would like to thank my advisor, Professor Jennifer Lewis: without her ideas and support this project would simply not exist, and her guidance has been crucial throughout my work. Professor Jacinta Conrad and Dr. Robert Shepherd were immensely important to this work, providing assistance and support throughout most of my graduate career. They taught me everything I know about working with colloidal materials and microfluidics, and were kind enough to answer many questions which I often could not even properly articulate. I owe special thanks to my undergraduate assistants, Alissa Cote, Stephen Menke, Fatima Salazar and Kundan Chaudhary: they all spent a lot of time on that microscope with me, and I can't imagine how I could have done without them. I would also like to thank the rest of the Lewis Group for many things, great and small and too numerous to mention, all of which made my life much easier; in particular Chris Hansen, John Vericella, David Lorang, Elizabeth Glogowski and Willie Wu. And Steve Kranz, who is taking over much of my work in the Lewis group, I thank and wish good luck.

As much as graduate school seems to be the entirety of one's life while it's going on, the rest of the world does in fact exist! With this in mind I would also like to extend thanks to those who transformed these years of my life into more than one long slog in the lab. Mom, Dad and Brian were my rocks, and more important than I can express without adding a second volume to this book. Dr. Huaibin Zhang was kind enough to give me fascinating things to work on when I wasn't busy with this thesis; and Max, Phil and Steve gave me games to play when I was done with that, too. The Lewis group as a whole have been more than just my colleagues, and I thank them all for much fun and merriment. Dorian, Moki, and Tink have been the truest friends I had when I needed them most, and deserve all the thanks and praise I can give them. And most of all I thank Leigh, without whom I would still be lost and alone in the woods. This is for you.

I know I've left people out, and to them I give my sincerest apologies. I could not list everyone without destroying the illusion that this work is, in fact, about colloids. The past few years have been hard and crazy and amazing, and I wouldn't trade them for anything. Thank you all.

Table of Contents

List of Figures

Chapter 1

Introduction

As a class of materials, self-assembled colloidal structures are of interest in applications as widely varied as photonic crystals **??**, photovoltaic devices **??**, and three-dimensional templates for tissue engineering scaffolds **??**. However, despite the wide interest in these structures, the range of possible structures made available by self-assembled spherical colloids is relatively narrow. Due to the isotropic nature of colloidal interactions, there are three basic structures available. **??** When the interparticle interaction is purely repulsive, such as in a hard-core interaction, two structures are available: a stable, ordered face-centered-cubic crystal structure(Fig. 1.1(a)) with a volume fraction of ??, and a dynamically-trapped disordered "glassy" state (Fig. 1.1(b)) with a slightly higher volume fraction of up to ??. Both of these structures are space-filling in the sense that there are no large gaps in the structure larger than the particle size. When the interparticle interaction is attractive, the particles may form an open, disordered "gel" structure (Fig 1.1(c)) with an essentially random arrangement and gap volumes which are potentially larger than the particle size **??**.

Many applications, such photonic crystals, would benefit from the availability of ordered structures with different geometries than fcc. One potential route for realizing different structures is to change the building block, replacing the isotropically-interacting spherical particles with some type of anisotropic particle. Here, we develop techniques for the fabrication of colliods with geometric and chemical anisotropy and begin to characterize the dynamical behavior and self-assembly of these particles.

1.1 Thesis Scope

The aim of this work is to develop techniques for the fabrication and characterization of anisotropic colloids, and begin to explore their dynamical and assembly characteristics. Fabrication is based on flow lithography techniques for producing polymeric particles **??**, and characterization is primarily based on fluorescence and

Figure 1.1: Spherical colloids with purely repulsive interactions may assemble into (a) ordered crystal structures with fcc geometry or (b) space-filling disordered "glass" structures. Attractive colloids assemble into (c) open "gel" structures.

confocal microscopy. The systems used are based on a combination of a hydrophobic monomer (tri(methylol propane) triacrylate) and hydrophilic monomers (poly(ethylene glycol) diacrylate and 20-mol ethoxylated tri(methylol propane) triacrylate). Single-component particles are used to study the effects of geometry on dynamical behavior in isolation, while multiple-component particles introduce the hydrophobic attraction for self-assembly. The solvents used are varied to explore this interaction, and include water, ethanol, dimethyl sulfoxide, isopropanol and toluene.

1.2 Thesis Organization

A review of the relevant literature on the fabrication of anisotropic colloids, their experimental and simulated self-assembly, and their characterization using particle tracking techniques is included in chapter two. Chapter three details algorithms and software developed in the course of this study to analyze microscopy images containing anisotropic colloids. Chapter four investigates the fabrication, behavior and self-assembly of simple rod-shaped colloids in both single-component and "Janus" forms, while chapter five investigates colloids with more exotic geometries. The main conclusions are presented in chapter six. Appendices are included which present experimental techniques developed for but not used in the final study, including novel microfluidic devices for studying concentrated colloids and a variant of the fabrication technique.

Chapter 2

Literature Review

2.1 Introduction

This literature review begins with an introduction to current work on the design and classification of anisotropic colloidal particles, and examples of real-world systems incorporating colloidal anisotropy. This is followed by a discussion of current techniques for the fabrication of anisotropic colloids, the theory of their self-assembly and experimental results. Flow lithography is then reviewed in detail to explore different forms of anisotropy which may be targeted by this technique. Finally we review the current state-of-the-art in the characterization of colloidal suspensions by particle tracking in microscopy image data, and potential extensions of this technique for tracking anisotropic particles.

2.2 Anisotropic and Patchy Colloids

2.2.1 Dimensions of Anisotropy

While the self-assembly of colloidal particles can produce structures with a variety of potential applications **??**, the range of structures which may be produced by conventional spherical colloids is limited. One way to address this is to introduce colloidal particles which incorporate one or more forms of anisotropy, in which the particle is altered such that the interaction between two or more particles becomes non-uniform depending on their relative orientations. These alterations may be based on the shape of the particles, the chemical makeup, or some combination of the two.

In a 2007 article in *Nature Materials* **??**, Glotzer and Solomon propose a system of anisotropy dimensions shown in Fig. 2.1. These include shape-based dimensions such as aspect ratio, faceting, branching, shape gradient and roughness (Fig. 2.1(B,C,E,G,H)) and dimensions based on the presence of multiple chemistries such as surface coverage, pattern quantization and chemical ordering (Fig. 2.1(A,D,G)). These dimensions do not necessarily represent an exhaustive list of the types of anisotropy which are theoretically possible, but are an observational list of anisotropy types which have been observed in the recent literature. For example, rod-

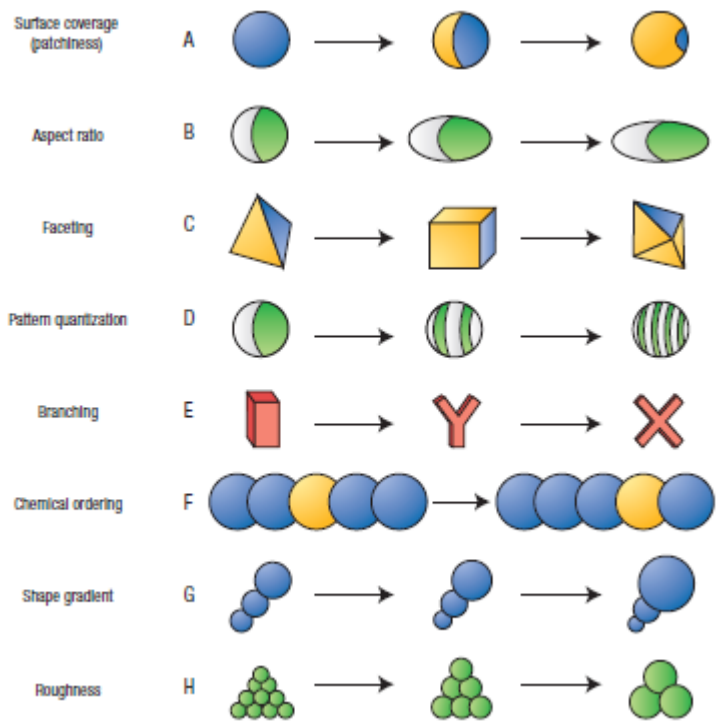

Figure 2.1: Anisotropy dimensions proposed by Glotzer and Solomon **??** to classify different forms of particle anisotropy.

shaped or ellipsoidal particles of moderate aspect ratio have been fabricated by a wide variety of techniques including lithography **??** and particle distortion **??**; branched tetrapods have been fabricated of gold **??** and CdTe **??**; and chemically patterned particles have been produced through microfluidic means **??** as well as by conventional photolithography **??**. This list of dimensions may therefore be seen as a useful framework for classification: by combining multiple dimensions, more complex types of particles may be developed (Fig. **??**), or a complex particle may be classified in terms of which dimensions it includes. New forms of anisotropy may be identified as those which cannot be decomposed into dimensions already identified.

As an example of a particle which combines many types of anisotropy, consider the "barcoded" particles described in *Tan et al.* **??** for DNA analysis (Fig 2.3). These particles have multiple aspect ratios (dimension B); faceting, due to the flat top and bottom surfaces (C); and pattern quantization due to the three different chemistries included (D). An additional form of anisotropy, the barcoding, may be seen as a new dimension or as a more complex instance of pattern quantization. While these particles are larger than typical colloidal dimensions, they illustrate these principles vividly and it is reasonable to suspect they may be miniaturized.

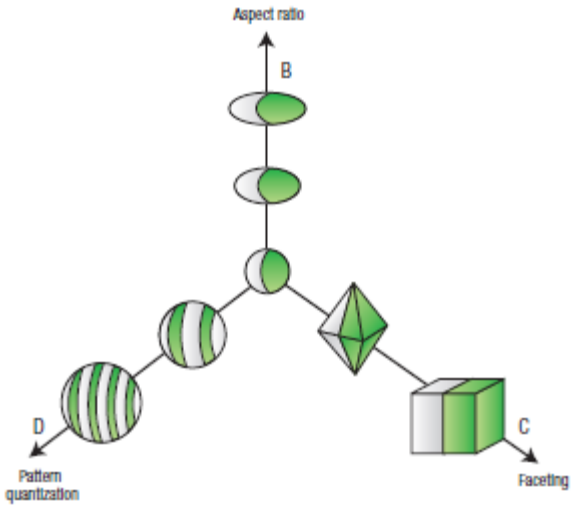

Figure 2.2: Multiple anisotropy dimensions may be combined to yield more complex types of particles. **??**

2.2.2 Theory of self-assembly

2.2.3 Fabrication of anisotropic colloids

- Fabrication of Janus spheres: Granick, etc
- Fabrication of rods
- Fabrication of Janus rods
- Faceted particles (crystal growth etc)
- Flow lithography
- PRINT particles
- Glotzer work on spherical patchy colloids
- Other self-assembly of spherical colloids
- Review self-assembly of non-spherical patchy colloids: focus on Janus rods

2.2.4 Experimental self-assembly

- Hydrophobic/hydrophilic: Granick, clusters
- Charge-based assembly

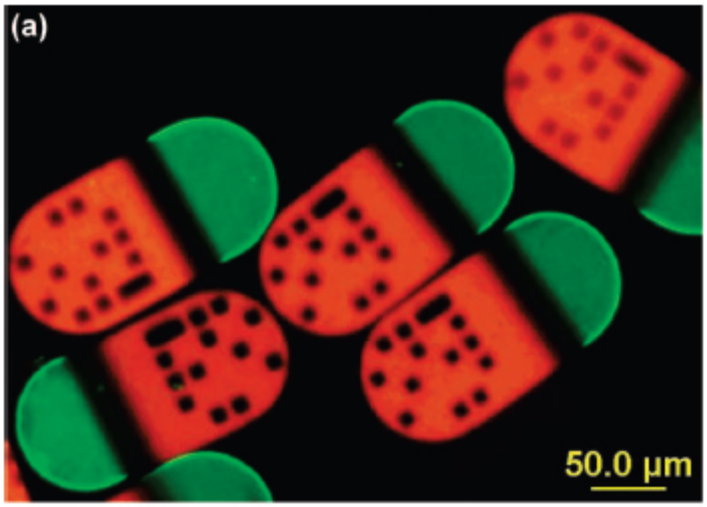

Figure 2.3: "Barcoded" PEG-DA particles which incorporating a DNA probe and fluorescent dyes **??**.

- Magnetic assembly
- DNA-based assembly

2.3 Flow Lithography

One technique for the fabrication of structured particles which has undergone active development in recent years is *flow lithography*, a technique developed by Patrick Doyle at MIT which combines microfluidics with UV lithography.

In a typical continuous flow lithography experiment, we construct a microfluidic device out of polydimethylsiloxane (PDMS) which contains a simple straight microchannel with cross-sectional dimensions between 5-400 μm. As a feedstock material we use some fast-photocuring low-viscosity liquid, typically a photocurable monomer solution. The device is placed on a microscope which includes some UV illumination source which may be reversed through the optical path (i.e. it is emitted at the objective lens) and a fast electronic shutter. A typical example might be a conventional fluorescence microscope with a mercury lamp. A photomask defining the particle geometry is placed at the microscope field stop so that it may shape the UV beam.

To fabricate particles, the photocurable liquid is pumped through the microchannel, and the microchannel

Figure 2.4: Janus spheres fabricated by emulsion technique **??**.

Figure 2.5: PMMA rods are fabricated by (a) embedding PMMA spheres in PDMS, (b) stretching the PDMS while heated and allowing it it to cool, and (c) dissolving the PDMS to reveal ellipsoidal rods.

is oriented parallel to the microscope's focal plane. The microscope objective is focused on a place inside the channel, and the electronic shutter is opened at intervals. If the UV light is intense enough and the liquid is moving at a slow enough speed, the UV-exposed region will cure into one or more solid particles. The flow of the liquid carries these particles out of the "active region", and provides fresh material.

The particle geometry is defined by a combination of the photomask and the microchannel. The two-dimensional cross-section is determined by the shape of the UV beam at its intersection with the microchannel, and the particle height is defined by the height of the microchannel. The "top" and "bottom" of the particles, where they meet the upper and lower microchannel surfaces, conform roughly to the shape of these surfaces and are generally flat. The particles may thus be viewed as 3D extrusions of the 2D mask. Friction or sticking with these top and bottom surfaces are prevented in the case where PDMS is the channel material and a hydrogel monomer is the feedstock: hydrogel curing is inhibited by the presence of oxygen, and PDMS is oxygen permeable. This results in the formation of an "inhibition layer" along the internal surfaces of the channel where the liquid will not cure, preserving the mobility of the particles. This layer is typically about 1 μmthick. The resolution and quality of the 2D pattern is affected by the focus of the microscope (defocusing will produce blurred boundaries), the resolution of the mask, and the magnification and numerical aperture of the objective lens.

2.3.1 Stop flow lithography

2.3.2 Multiple-component FL

2.4 Particle Tracking

- Crocker and Grier: IDL particle tracking
- Solomon: rod particle tracking
- Other relevant tracking?
- Basic review of morphological image processing

Figure 2.6: Small clusters of Janus spheres; wormlike chains; Granick

Figure 2.7: Multi-panel figure: other assembly

Figure 2.8: Particle tracking illustration

Figure 2.9: Solomon rod tracking

Figure 2.10: Illustrate morphological processing

Chapter 3

Computerized Tracking of Anisotropic Colloids

3.1 Introduction

Confocal laser scanning microscopy (CLSM) is a powerful technique for the study of three-dimensional structure in fluorescent materials. When applied to fluorescent colloids, CLSM enables the observation and identification of individual particles, determining their positions in three-dimensional space. These particle locations alone can be used to derive a great deal of information about the material, such as the distribution of number of nearest neighbors and the pair distribution function (PDF). Repeated observations at regular intervals allow for dynamical measurements of parameters such as the diffusion constant, and may be used to study the microstructual differences between different parts of the colloidal phase diagram. CLSM has the additional advantage that since it produces real-space position data, it has substantial advantages over scattering techniques in coping with samples with highly asymmetric structures. **??**

However, the production of 3D structural information requires more than just a powerful imaging technique: it also requires powerful computational analysis to translate image data into a list of particles and positions, and to determine the relevant physical data from this list. In addition, the behavior of non-spherical colloids is governed not only by the relative positions of the particles but also their orientations. Developing an understanding of anisotropic colloids therefore calls for the development of image processing techniques for the extraction and analysis of structural data from microscopy images.

3.2 Literature review

3.2.1 Particle tracking with spherical colloids

The current state of the art in

3.2.2 Solomon rod tracking

- Desirable to locate anisotropic particles in microscopy images to study dynamics and assembly.

Figure 3.1: Illustration of Solomon technique

Figure 3.2: SFL particles as 2D extruded objects; flat fluorescence

- Previous work in this area: Crocker and Grier, Solomon
- Can't use Solomon method: fluorescence is too flat for SFL particles. 2D-extruded objects. (Figure to illustrate.)
- Must develop new algorithms which can work on these particles.

3.3 Rod-tracking algorithm

Our algorithm for locating and tracking SFL rods draws heavily from the algorithm published by Mohraz and Solomon for tracking PMMA rods. **??**. Briefly, this algorithm took advantage of the gradient in fluorescent intensity throughout the volume of the rods they studied, which were fabricated by stretching spherical PMMA particles along a single axis. Because these rods had a circular cross-section, scanning the confocal laser through a point nearer to the rod axis would pass through a greater volume of fluorescent material, producing a higher intensity. By applying a local line maximum criterion to the points inside the particle volume, they were able to build a "backbone" of points near the axis, allowing them to reliably calculate orientation.

While this algorithm performs very well for a restricted class of rods, it fails in cases where the particle cross-section is not circular, and points near the particle backbone are not guaranteed to produce higher intensities than their immediate neighbors. This is the case for our "rods" produced by stop-flow lithography (SFL), in which the sides of the rods are relatively flat due to the fabrication geometry. These particles have correspondingly flat fluorescence profiles, and require a more complex analysis to calculate a "backbone".

We have developed an algorithm for processing 2D and 3D CLSM data of fluorescent SFL rods to produce position and orientaion data. Starting from raw CLSM images, this algorithm can be divided into several phases, including (i) image cleanup; (ii) segmentation; (iii) skeletonization; (iv) position calculation; and (v) particle tracking over the time series.

A note on terminology: the algorithm described below is identical for both 2D and 3D images, as all operations are defined for both cases and used identically. However, where the individual elements of 2D images are referred to as pixels, the elements of 3D images are generally referred to as voxels. For simplicity, all such elements are referred to as pixels in the explanation below.

3.3.1 Image cleanup

Two different image cleanup methods were considered, and used depending on their effectiveness with sample data.

The first method, a real-space bandpass filter, is derived from the filter published in the Matlab implementation of spherical particle tracking **??** by Blair and Dufrense. This filter performs a band-pass by convolving the image with two kernels: a Gaussian kernel and a boxcar kernel. The Gaussian convolution performs the low-pass operation, while subtracting the result of the boxcar convolution from the Gaussian result performs the high-pass operation. This filter takes two parameters, the characteristic scale of image noise (generally equal to one pixel) and the typical particle size. This works well, but has issues in images with multi-pixel noise.

While the band-pass performed well on most images, some experiments produced data with noise or extraneous features which did not easily yield to the bandpass operation. This can be attributed to the fact that SFL fabrication produces solutions which have some amount of fluorescent monomer present in the liquid as well as the particles, which could not always be removed effectively. A second method was devised using morpholohical operations to better neutralize non-particle features.

This method may be divided into four steps. First the image is thresholded to produce a binary image, where the background is black and the fluorescent features are white. The threshold is selected such that pixels which are part of the particle volume are never assigned to the background; Otsu's criterion was found to be reliable for this. **??** Second, a binary opening is applied with an isotropic structuring element to suppress small features. The size of the structuring element is selected manually by the user, but a reliable choice was found to be a diameter roughly equal to half the width of the typical rod.

At this point a binary image has been produced which suppresses most non-particle features, but morphological image operations are not guaranteed to preserve shape and orientation of image features. To retain the noise suppresion but regain the original shape, we perform one additional morphological dilation using the same structuring element to guarantee that the foreground regions fully overlap with the rods, then perform a binary AND between the result and the original image. This is effectively equivalent to using the result of our morphological operations as a mask on the original, suppressing all pixels which are marked as background.

3.3.2 Segmentation

The next step of the algorithm is image segmentation, in which individual particles are identified and each pixel in the image is assigned to a specific particle, or to the background. This is especially important in

the study of Janus rods, which are come into contact during self-assembly and which therefore often touch or overlap in CLSM images.

First, the image is thresholded to produce a binary image, with a threshold selected such that all pixels which are part of the rods are assigned to the foreground. This may generally be accomplished through the use of Otsu's criterion. **??**

Second, the distance transform is calculated. In this step, each foreground pixel is assigned a number which gives the distance between this pixel and the nearest background pixel. In this algorithm, the distance measure used is simple Euclidean distance, calculated center-to-center between this pixel and the closest background pixel. Alternative distance measures such as the "chessboard" measure may also be used to speed up computation, but these measures were found to negatively impact segmentation. To prepare the image for watershed segmentation, the distance transform is transformed such that all distances are made negative, while the background remains at a flat zero. An h-minima transform is applied to remove small local minima due to noise in the image.

The primary segmentation step is the watershed transform. In this transform, a gray-level image is viewed as a topographic relief map where the pixel values represent altitude. A drop of water falling on a relief surface will run down to a minimum, and many drops will fill any basins present until the basins merge. Implementations of the watershed transform use this concept to calculate the boundaries between catchment basins, fully segmenting the image. The number of basins is calculated either by using local minima in the image, or by pre-assigning a set of markers. In our algorithm, we generally use the Matlab implementation of `watershed` which uses the local minima method. This carries some danger of over-segmentation (mitigated somewhat by the h-minima transform), but is better suited to automatic processing of a large number of images than manual markers.

`watershed` outputs an image which labels each pixel according to a region ID number, and labels both background and foreground pixels with these regions. To restrict these labels so that the background is labeled separately, all watershed pixels which correspond to background-valued pixels in the thresholded image are assigned a label number of zero.

3.3.3 Skeletonization

Once we have identified which image pixels belong to each particle, we need to put this data into a form from which reliable position and orientation information can be calculated. While it is tempting to simply calculate the centroid and associated moments from the raw pixel data, this can be problematic when working with time-series data due to boundary noise. Consider a single foreground pixel belonging to an identified

particle which is experimentally constrained to be stationary, and which is adjacent to a background pixel because it is on the edge of the identified region. In the next image in the time series, this pixel's intensity is reduced and it is identified as a background pixel. If we are calculated particle position as the average of all the identified pixels, this will result in the calculated position changing, even if the particle did not physically move. The next frame after that, it may be re-identified as a foreground pixel. While the effect is small, experimental conditions may magnify these effects and produce appreciable fluctuations in the position and orientation. One way to get around this issue is to calculate a particle "skeleton" which is less sensitive to this form of noise.

For a rod, we calculate a backbone very similar to the backbone calculated in the Mohraz-Solomon algorithm; but rather than using an intensity gradient, we instead calculate with respect to the particle geometry. For each particle, we calculate the distance transform and apply a local line maximum constraint. The line maximum constraint is applied for eight line orientations, and the pixel is considered a backbone pixel if a certain number of these are satisfied (typically 50%).

3.3.4 Calculation of position and orientation

3.3.5 Particle tracking

Figure 3.3: Image processing flowchart

Figure 3.4: Example image: cleanup, segmentation, skeleton, track

Figure 3.5: Schematic comparison of 2D/3D

- Tracking algorithm for arbitrary shapes
  - Initial steps same as for rods: cleanup, segmentation
  - "Skeletonization" as above, but producing a more complex skeleton than for rods
  - Calculate center-of-mass as with rods
  - Choose a sample skeleton as the "canonical" particle skeleton
  - Isolate particles into individual windows
  - To measure orientation: rotate canonical skeleton image in small increments. For each one, AND together the rotated skeleton and the sample skeleton. Maximize pixel sum of ANDed image.

Figure 3.6: Schematic explanation of "template" technique for tracking arbitrary shapes

Figure 3.7: Example images for "template" tracking

- Faster in 2D than in 3D
- Implementation not finished!

3.4 Implementation

Figure 3.8: Example particle tracks

- Rod tracking implemented in 2D in Matlab.
- Go over the details of the matlab implementation
- Rod tracking implemented in 3D in Matlab, but with major bugs.
- Arbitrary tracker not yet fully implemented, using Matlab.

3.5 Assessment

- Identify issues caused by morphological image processing for these algorithms.
- Estimate errors in particle segmentation
- Estimate error of rod COM and orientation calculations.
- Estimate error of skeleton-based orientation calculations.

Figure 3.9: Cartoons to show possible errors

Chapter 4

Assembly and Dynamics of Rod-Shaped Colloids

4.1 Introduction

Figure 4.1: Colloidal rod examples

- Natural rod systems
- Systems studied by Solomon
- Janus colloids: Granick
- Interest in Janus rods

4.2 Experimental Procedure

4.2.1 Stop-Flow Lithography

Figure 4.2: Photo of SFL setup; SFL flowchart; example experiment

- Microscope setup
- Pressure system–Rob
- LabView controller for SFL
- Design of microfluidic devices for up to 3-stream SFL
- Fabrication of microfluidic devices

Figure 4.3: Examples of SFL masks used in rod experiments

4.2.2 Mask Design

- Demagnification using 60X objective
- Design parameters
- Rod aspect ratios used

4.2.3 Particle Collection

- Considerations for collection
- Solvents used
- Pipettes
- Fluorosilane coatings

4.2.4 Diffusion Measurements

- Confocal microscopy setup
- Space and time resolution requirements
- Fluorescence requirements

4.3 Results and Discussion

Figure 4.4: Resolution test mask; image of resulting particles

4.3.1 Resolution

- Limiting factors for SFL resolution: mask design, optics, flow effects
- Resolution limits constrained by 60X lens–need to redo this (1 hour work)
- Resolution limits for Janus rods–interface effects

Figure 4.5: Image of rod tracking

Figure 4.6: Plots of translational and rotational diffusion data

4.3.2 Translational and Rotational Diffusion

- Particle collection–PEGDA vs TMPTA
- Compare particle/solvent/surface effects
- 2D diffusion size series: TMPTA in toluene (additional experiments may be required)
- Analyze diffusion data for rods (partially done).

Figure 4.7: Show fabricated Janus rods of various sizes.

Figure 4.8: Assembly of rods in various solvents

4.3.3 Self-Assembly of Janus Rods

- Fabrication of Janus rods: various sizes (figure)
- Comparison of self-assembly in various solvents (figure)
- Small clusters vs large structures
- Alignment of assembled rods
- Image segmentation for analyzing structures
- Some more good-looking images may be required

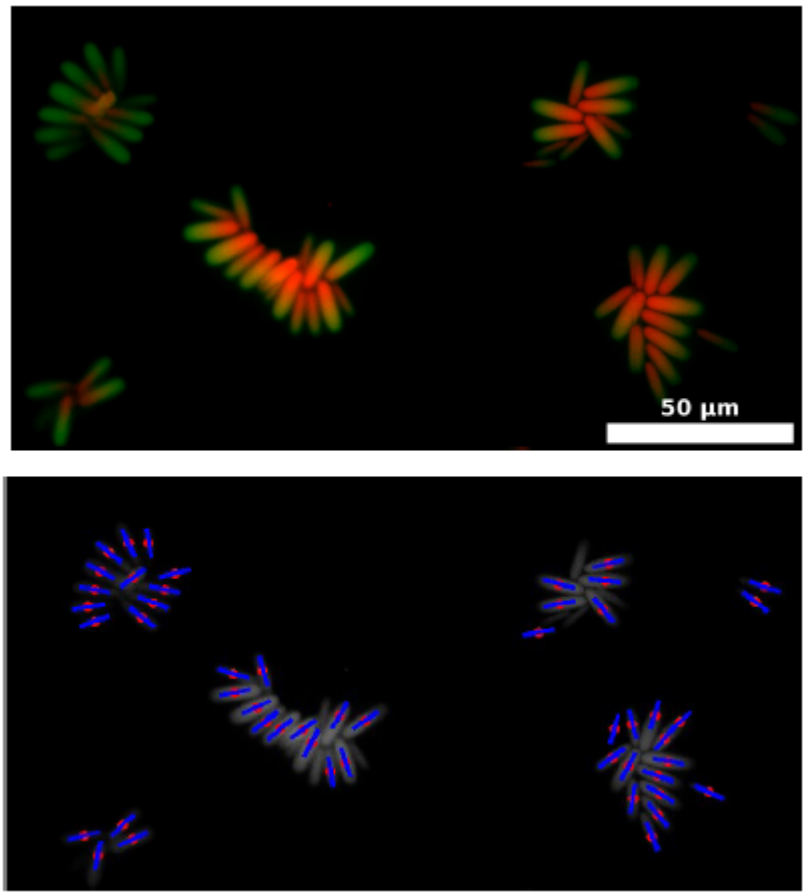

Figure 4.9: (a) Janus rods which have self-assembled into ordered clusters are identified and separated, and (b) their positions and orientations are labeled.

Chapter 5

Assembly and Dynamics of Exotic Colloids

5.1 Introduction

Figure 5.1: Glotzer anisotropy dimensions targeted by complex SFL

- Motivation for working on more complex shapes
- Reference Glotzer anisotropy dimenions
- Bring back three-stream SFL concept from lit review

5.2 Experimental Procedure

5.2.1 Device Design

Figure 5.2: Schematic for 3-stream channel, and constriction channel

- Design for three-stream SFL microfluidic device: explain considerations
- Channel-constriction design

5.2.2 SFL with Multiple Co-Flowing Streams

- **Alterations necessary to SFL protocol with three streams**
  - Timing considerations
  - Pressure considerations

5.3 Results and Discussion

5.3.1 SFL limitations

Figure 5.3: Show stable parallel interface vs droplet forming

- Multiple streams result in SFL slowdown
- Theoretical constraints on how closely interfaces can be spaced
- Empirical comparsion on interface spacing

5.3.2 Particles produced

Figure 5.4: Figure showing 2, 3, 4 patch particles

Figure 5.5: Figure showing boomerangs, and self-assembly concept

- Family of particles produced
- Branched (multi-patch) particles (figures)
- Boomerang fabrication and concept

5.3.3 Diffusion Measurements

- Confocal measurements of 2D diffusion for various shapes–not systematically done
- Diffusion results

5.3.4 Self-Assembly

- Some self-assembly observed for two-patch rods
- Little self-assembly observed for larger, less mobile particles
- Surface effects may affect observed assembly

Figure 5.6: Diffusion results for complex particles

Figure 5.7: Show two-patch self-assembly

Figure 5.8: Show samples with little assembly; schematic of surface effects

Chapter 6

Conclusions

- Fabrication of shape and chemical anisotropic colloids by stop-flow lithography
- Computer-based tracking of rod-shaped colloids
- Computer-based tracking of arbitrary-shaped colloids
- Fabrication of Janus rods
- Demonstrated self-assembly of Janus rods
- Fabrication of more complex colloids

6.1 Future work

- Microfluidic devices to study self-assembly (see appendix)
- High-concentration studies
- Mixtures of spherical and non-spherical colloids

Appendix A

Microfluidic Devices for Studying Self-Assembly

A.1 Introduction

- SFL is low-scale technique for fabricating very small particles
- Most interesting physics occurs at higher concentrations
- SFL yields are low once particles are transferred out of device
- Single microfluidic system to fabricate and study particles is desirable

A.2 Experimental Procedure

A.2.1 Device Design and Fabrication

Figure A.1: Overall design

Figure A.2: Post filters; Channel-height filters

- Design capable of multi-stream fabrication
- Design capable of concentrating particles in a small container
- Multi-layer SU-8 master fabrication
- Initial filter design: posts
- Final filter design: channel height
- Concentrator geometries
- System to exchange solvents and clean particles

A.2.2 Proposed Protocol

Figure A.3: Cartoon of proposed protocol

- Fabricate particles in channel
- Particles collect in concentration chamber
- When finished, cure fab channel shut
- Rinse particles
- Agitate to break up structure
- Image

A.3 Results and Discussion

A.3.1 Concentrator results

Figure A.4: Janus particles in concentrator

Figure A.5: Failed devices

- Particle fabrication: slowed by pressure
- Particle concentration by filters
- Solvent exchange: challenges due to pressure buildup
- Aggregates refuse to break up: suggested explanations
- Device failures

A.4 Future directions

- Suggestions on device design
- Suggestions for other uses of these devices

Appendix B

Grayscale Stop-Flow Lithography

B.1 Introduction

- SFL particle height set by channels; low versatility
- Allow height variation within channel?
- Give examples of grayscale lithography

B.2 Experimental Procedure

B.2.1 Design of Grayscale Filters

Figure B.1: Plot transmission vs filter thickness

- Construct mixed-PDMS filters

B.2.2 Grayscale Stop-Flow Lithography

Figure B.2: Cartoon of grayscale SFL fabrication

- Placement in SFL beam path
- Experimental optimization

B.3 Results and Discussion

B.3.1 Resulting particles

- Achieved height variation

- Particle swelling issues observed

B.4 Future work

- True grayscale masks